Kondo Lattice Model in Magic-Angle Twisted Bilayer Graphene

Yang-Zhi Chou* and Sankar Das Sarma
Condensed Matter Theory Center and Joint Quantum Institute, Department of Physics, University of Maryland, College Park, Maryland 20742, USA

(Received 25 December 2022; accepted 2 June 2023; published 11 July 2023)

We systematically study emergent Kondo lattice models from magic-angle twisted bilayer graphene using the topological heavy fermion representation. At the commensurate fillings, we demonstrate a series of symmetric strongly correlated metallic states driven by the hybridization between a triangular lattice of $SU(8)$ local moments and delocalized fermions. In particular, a (fragile) topological Dirac Kondo semimetal can be realized, providing a potential explanation for the symmetry-preserving correlated state at $\nu = 0$. We further investigate the stability of the Dirac Kondo semimetal by constructing a quantum phase diagram showing the interplay between Kondo hybridization and magnetic correlation. The destruction of Kondo hybridization suggests that the magic-angle twisted bilayer graphene may be on the verge of a solid-state quantum simulator for novel magnetic orders on a triangular lattice. Experimental implications are also discussed.

DOI: 10.1103/PhysRevLett.131.026501

Introduction.—Magic-angle twisted bilayer graphene (MATBG) [1,2] has been a promising platform to study strongly correlated phases because the nearly flat bandwidth [3] effectively enhances many-body interactions. Recent experiments [1,2,4–17] have shown abundant phenomena such as correlated insulators, superconductivity, quantum anomalous Hall effect, and flavor polarization. One of the unsettled experimental issues is the seeming contradiction between transport and STM measurements at the charge neutrality point ($\nu = 0$). Several transport experiments [1,2,4,15] found semimetallic behavior at $\nu = 0$, which can be described by the noninteracting Bistritzer-MacDonald (BM) model [3]. However, STM measurements [9,10,14,17] observed strong local correlations at $\nu = 0$, indicating significant interactions. Thus, it is natural to ask if a potential mechanism exists explaining both transport and STM experiments.

Studying interaction-driven phenomena in MATBG is technically challenging because the two flat bands belong to the fragile topological states protected by a $\mathcal{C}_{2z}\mathcal{T}$ symmetry [18–20], implying the absence of a lattice model description for the flat bands. Recently, Song and Bernevig proposed a novel topological heavy fermion (THF) representation [21], reconstructing the MATBG flat bands by coupling localized orbitals (f fermions) and delocalized topological conduction bands (c fermions). Notably, the localized f fermions can be viewed as the zeroth pseudo-Landau levels located at the AA stacking registries [22,23]. Song and Bernevig further demonstrated that this THF representation is advantageous for studying interaction-driven phases because the one-shot Hartree-Fock results qualitatively capture the essence of self-consistent Hartree-Fock calculations [21], suggesting a good starting point for exploring strongly correlated physics in MATBG.

In this Letter, we construct and study Kondo lattice models for MATBG using the newly developed THF model [21,23]. The f orbitals can be viewed as SU(8) local moments when the onsite Hubbard interaction is sufficiently large. We show that a series of symmetry-preserving correlated metallic states arise naturally from the hybridization between the SU(8) local moments (spin, valley, and orbital) and the delocalized c fermion. In particular, a fragile topological Dirac Kondo semimetal is realized at $\nu = 0$, providing a potential resolution for both the transport and STM measurements at $\nu = 0$. This prediction is distinct from the existing Hartree-Fock studies [21,23–31]. To examine the stability of the Dirac Kondo semimetal state, we consider Heisenberg interaction among the nearest-neighbor local moments and construct a quantum phase diagram. One interesting implication is that MATBG might be on the verge of a SU(8) Heisenberg model on a triangular lattice, paving an unprecedented way for studying exotic magnetic phases in solid-state systems.

Model.—We are interested in the MATBG low-energy bands with strong correlations. The single-particle dispersion is well described by the BM model [3]. Here, we adopt a new alternative strategy using the THF representation [21,23]. The main idea is that the low-energy MATBG bands can be reconstructed by coupling localized orbitals (at zero energy) and delocalized topological bands. The localized orbitals (f fermions) live on a triangular lattice with the lattice constant a_M being the

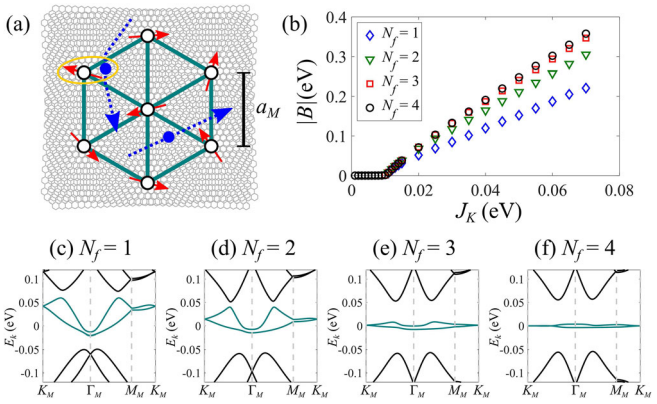

FIG. 1. Kondo lattice model for MATBG. (a) The real-space structure. Local moments (red arrows) are located at the AA stacking registries and form a triangular lattice with a lattice constant a_M. The delocalized c fermions (blue dots) interact with these local moments. (b) The Kondo hybridization amplitude as a function of J_K with different values of N_f. The results are obtained by solving Eqs. (6)–(8) with a 30×30 momentum mesh in each mBZ. (c)–(f) Quasiparticle dispersion of $\eta = +1$ for $J_K = 0.03$ eV with different N_f. $(\nu_f, \nu_c) = (N_f - 4, 0)$ in these plots. The mini bands are highlighted with green.

moiré period as shown in Fig. 1(a); the delocalized bands (c fermions) travel in continuous space, described by [21]

$$\hat{H}_{0,c} = \sum_{\eta,s,a,a'} \sum_{\mathbf{q}} h^{(\eta)}_{aa'}(\mathbf{q}) c^{\dagger}_{\mathbf{q},a,\eta,s} c_{\mathbf{q},a',\eta,s}, \tag{1}$$

where $\hat{h}^{(\eta)}(\mathbf{q})$ is a 4×4 matrix dictating the delocalized bands [32], $c_{\mathbf{q},a,\eta,s}$ is the annihilation operator for the delocalized bands with valley η, spin s, orbital a ($a = 1, 2, 3, 4$), and is a wave vector $\mathbf{q}$. Since c fermions can travel in the continuous space freely (i.e., not trapped by the triangular lattice points), they can carry wave vectors outside of the first moiré Brillouin zone (mBZ) defined by the triangular superlattice. The hybridization between c and f fermions is described by [21]

$$\hat{H}_{0,cf} = \sum_{\eta,s,\alpha,a} \sum_{\mathrm{G}} \sum_{\mathbf{k}\in \mathrm{mBZ}} \left[V^{(\eta)}_{\alpha a}(\mathbf{k}+\mathbf{G}) f^{\dagger}_{\mathbf{k},\alpha,\eta,s} c_{\mathbf{k}+\mathbf{G},a,\eta,s} + \mathrm{H.c.} \right], \tag{2}$$

where $V^{(\eta)}_{\alpha a}(\mathbf{q})$ is a 2×4 matrix [32], $f_{\mathbf{k},\alpha,\eta,s}$ is the annihilation operator for the localized orbital with orbital α ($\alpha = 1, 2$), valley η, spin s, and wave vector $\mathbf{k}$ defined in the first mBZ, and $\mathbf{G}$ is the reciprocal lattice vector of the triangular superlattice. The characteristic single-particle hybridization is $\gamma = -24.75$ meV, and $|\gamma|$ controls the distance between the low-energy and remote bands [21]. Equation (2) conserves only the crystal momentum. Thus, the f fermion with wave vector $\mathbf{k}$ couples to all the c fermions with wave vectors $\mathbf{k} + \mathbf{G}$ for all the allowed $\mathbf{G}$. In our calculations, we consider a finite number (N_G) of reciprocal lattice vectors. $N_G = 37$ is used for all the results.

In addition to the single-particle part, the Coulomb interaction can be projected into the THF basis [33], and the interacting part of the Hamiltonian is given by $\hat{H}_I = \hat{H}_U + \hat{H}_V + \hat{H}_W + \hat{H}_J$ [21], where

$$\hat{H}_U = \frac{U}{2} \sum_{\mathbf{R}} (\hat{\rho}^f_{\mathbf{R}} - 4)^2 \tag{3}$$

describes the on-site repulsive interactions ($U > 0$) among the f fermions [34], $\hat{H}_V$ denotes the Coulomb interaction between c fermions. $\hat{H}_W$ is the density-density interaction between f and c fermions (similar to the interaction in the Falicov-Kimball model), and $\hat{H}_J$ is a U(4) Hund's rule coupling. In Eq. (3), the subtraction of 4 incorporates the effect of the ionic charge background.

To study the interacting MATBG, we make a few simplifications [33]. We ignore the $\hat{H}_V$ term because it mostly renormalizes the c fermion dispersion (e.g., band velocity and chemical potential) but unlikely induces any qualitatively change in the results. We also neglect the $\hat{H}_W$ term as it primarily gives shifts of chemical potentials. While $\hat{H}_J$ is crucial for stabilizing correlated insulating states in Hartree-Fock calculations [21], it is irrelevant to the symmetric Kondo correlated metals within the mean-field treatment as we discussed in the Supplemental Material [32]. Since we focus only on the Kondo-driven phases, the minimal interacting model for MATBG is described by $\hat{H}_{0,c} + \hat{H}_{0,cf} + \hat{H}_U$ [Eqs. (1)–(3)].

Kondo lattice and heavy fermion phase.—The Hamiltonian $\hat{H}_{0,c} + \hat{H}_{0,cf} + \hat{H}_U$ can be viewed as a periodic Anderson model [35,36] for MATBG. When U is sufficiently strong (i.e., $U \gg |\gamma|$), the local occupation number of f fermions (N_f) is frozen at each site. In such a situation, the cf hybridization ($\hat{H}_{0,cf}$) is inert, and a Kondo coupling emerges at the second order of $\hat{H}_{0,cf}$ [35,36] (see Supplemental Material [32]),

$$\begin{aligned} \hat{H}_K = & \frac{J_K}{\mathcal{N}_k \gamma^2} \sum_{\substack{\alpha,\eta,a,s \\ \alpha',\eta',a',s'}} \sum_{\mathbf{G},\mathbf{G}'} \sum_{\mathbf{k},\mathbf{k}'} \sum_{\mathbf{R}} \left[V^{(\eta')}_{\alpha' a'}(\mathbf{k}'+\mathbf{G}') \right]^* V^{(\eta)}_{\alpha a}(\mathbf{k}+\mathbf{G}) \\ & \times e^{i(\mathbf{k}-\mathbf{k}')\cdot\mathbf{R}} : f^{\dagger}_{\mathbf{R},\alpha,\eta,s} f_{\mathbf{R},\alpha',\eta',s'} : : c^{\dagger}_{\mathbf{k}'+\mathbf{G}',a',\eta',s'} c_{\mathbf{k}+\mathbf{G},a,\eta,s} : \hat{\mathcal{P}}_{N_f}, \end{aligned} \tag{4}$$

where $:A:$ denotes the normal order of A [37], and $\hat{\mathcal{P}}_{N_f}$ is the projection operator onto the subspace with exactly N_f localized f fermions per site. In the above expression, the Kondo coupling has a nontrivial momentum dependence. In a limit that $\mathbf{k} + \mathbf{G} \to 0$ and $\mathbf{k}' + \mathbf{G}' \to 0$, $[V^{(\eta')}_{\alpha' a'}(0)]^* V^{(\eta)}_{\alpha a}(0)$ is reduced to $\gamma^2 \delta_{a',\alpha'} \delta_{a,\alpha}$, and Eq. (4) becomes to a SU(8) Coqblin-Schrieffer coupling [35,36,38] with a coupling

constant J_K. Using $U = 57.95$ meV (the same value used in Ref. [21]), we obtain $J_K \approx 42.28$ meV, indicating that J_K cannot be ignored. In addition, the value of J_K is insensitive to N_f [32]. We emphasize that $\hat{H}_K$ and $\hat{H}_J$ act on different orbital subspaces of c fermions, so they should be treated separately.

To study the Kondo lattice model $\hat{H}_{0,c} + \hat{H}_K$, we employ the Read-Newns decoupling [35,36,39] (i.e., hybridization decoupling). The main results are summarized in the main text, and the derivations can be found in Supplemental Material [32]. In the mean-field theory, the $\hat{H}_K$ is replaced by

$$\hat{H}_K \to \sum_{\substack{\eta,s\\ \alpha,a}} \sum_{\mathbf{G}} \sum_{\mathbf{k}\in \mathrm{mBZ}} \left[\frac{B}{\gamma} V^{(\eta)}_{\alpha a}(\mathbf{k}+\mathbf{G}) f^\dagger_{\mathbf{k},\alpha,\eta,s} c_{\mathbf{k}+\mathbf{G},a,\eta,s} + \mathrm{H.c.} \right] + \sum_{\mathbf{k}\in \mathrm{mBZ}} \frac{|B|^2}{J_K}, \tag{5}$$

where the Kondo hybridization

$$B = -\frac{J_K}{\mathcal{N}_k} \sum_{\mathbf{G}} \sum_{\mathbf{k}\in \mathrm{mBZ}} \sum_{\alpha,\eta,s} \frac{V^{(\eta)}_{\alpha a}(\mathbf{k}+\mathbf{G})}{\gamma} \left\langle f^\dagger_{\mathbf{k},\alpha,\eta,s} c_{\mathbf{k}+\mathbf{G},a,\eta,s} \right\rangle, \tag{6}$$

and $\mathcal{N}_k$ is the number of $\mathbf{k}$'s in the first mBZ (equivalent to the number of lattice points). This mean-field decoupling is asymptotically valid for a SU(N) system with $N \gg 1$ [35,36]. We use the same mean-field decoupling for $\hat{H}_J$ and find that $\hat{H}_J$ vanishes exactly as long as the states are symmetric in valleys and orbitals [32]. This technical observation indicates that $\hat{H}_J$ is not essential for the Kondo lattice problems without valley or orbital symmetry breaking.

Finally, we need to impose a local constraint such that each site contains exactly N_f f fermions. In the mean-field treatment,

$$\frac{1}{\mathcal{N}_k} \sum_{\mathbf{k}\in \mathrm{mBZ}} \sum_{\alpha,\eta,s} \left\langle f^\dagger_{\mathbf{k},\alpha,\eta,s} f_{\mathbf{k},\alpha,\eta,s} \right\rangle = N_f. \tag{7}$$

Similarly, we can compute the number of c fermions per site with a finite N_G (the number of mBZs included),

$$\frac{1}{\mathcal{N}_k} \sum_{\mathbf{G}} \sum_{\mathbf{k}\in \mathrm{mBZ}} \sum_{a,\eta,s} \left\langle c^\dagger_{\mathbf{k}+\mathbf{G},a,\eta,s} c_{\mathbf{k}+\mathbf{G},a,\eta,s} \right\rangle = N_c. \tag{8}$$

The total filling is determined by $\nu = \nu_f + \nu_c$, where $\nu_f = N_f - 4$ and $\nu_c = N_c - 8N_G$. Assuming that the interaction effect is dominated by the f fermions [21,23], we treat the integer fillings as $\nu = \nu_f$ and $\nu_c = 0$. For a noninteger filling, one needs to compute the zero-point energy (i.e., contributions from $\hat{H}_V$ and $\hat{H}_W$ [21], which we ignore) to determine the precise ν_f and ν_c.

The mean-field action in the imaginary-time path integral is given by [32]

$$\mathcal{S}_{\mathrm{MF}} = \frac{1}{\beta} \sum_{\omega_n} \sum_{\eta,s} \sum_{\mathbf{k}\in \mathrm{mBZ}} \hat{\bar{\Psi}}^{\eta,s}_{\omega_n,\mathbf{k}} \left[-i\omega_n + \hat{\mathcal{H}}^{\eta,s}(\mathbf{k}; B, \mu_c, \mu_f) \right] \hat{\Psi}^{\eta,s}_{\omega_n,\mathbf{k}} + \beta \mathcal{N}_k \left(\frac{\mathcal{B}^2}{J_K} + \mu_f N_f + \mu_c N_c \right), \tag{9}$$

where $\hat{\mathcal{H}}^{\eta,s}$ is a $(2+4N_G) \times (2+4N_G)$ matrix, $\hat{\Psi}^{\eta,s}_{\omega_n,\mathbf{k}}$ is a $(2+4N_G)$-component field made of $f_{\mathbf{k},\alpha,\eta,s}$ as well as $c_{\mathbf{k}+\mathbf{G},a,\eta,s}$, and μ_f (μ_c) is the chemical potential for f (c) fermions. We can straightforwardly show that the self-consistent equations given by Eqs. (6)–(8) are equivalent to the saddle-point equations. Within the saddle-point approximation [35], the mean-field energy per site can be derived by integrating out the fermionic fields and taking the zero-temperature limit:

$$\frac{E_{\mathrm{MF}}}{\mathcal{N}_k} = \frac{1}{\mathcal{N}_k} \sum_{\mathbf{k}\in \mathrm{mBZ}} \sum_{\eta,s} \sum_{b=1}^{2+4N_G} \mathcal{E}^{\eta,s}_b(\mathbf{k}) \Theta[-\mathcal{E}^{\eta,s}_b(\mathbf{k})] + \left(\frac{|B|^2}{J_K} + \mu_f N_f + \mu_c N_c \right), \tag{10}$$

where $\mathcal{E}^{\eta,s}_b(\mathbf{k})$ is the eigenvalue of $\hat{\mathcal{H}}^{\eta,s}(\mathbf{k}; B, \mu_c, \mu_f)$ and $\Theta(x)$ is the Heaviside function.

To obtain the mean-field ground state, we numerically solve the self-consistent equations given by Eqs. (6)–(8) [32]. Then, we compute the E_{MF} [Eq. (10)] of all the solutions. The ground state is the solution with the minimal E_{MF}. For $\nu_f = \nu_c = 0$, μ_c and μ_f are exactly zero, so the self-consistent procedure can be greatly simplified. For general cases, one has to choose the correct values of μ_f and μ_c so that Eqs. (7) and (8) are satisfied. Remarkably, for $N_f \neq 4$, μ_f obtained from solving self-consistent equations can be significantly different from the local chemical potential for deriving $\hat{H}_K$ [Eq. (4)], suggesting that the local chemical potential is strongly renormalized. We choose a gauge corresponding to $B < 0$, and the results are not affected by such a choice [35]. The detailed numerical procedures are discussed in Supplemental Material [32].

Now, we construct a phase diagram for the Kondo hybridization formation. In Fig. 1(b), we plot $|B|$ as a function of J_K for different N_f with $\nu_c = 0$. The results suggest a threshold around $J_K = 0.01$ eV, above which $|B|$ becomes finite. For $J_K < 0.01$ eV, we conclude that $|B| \to 0$ based on finite-size analysis [32]. The filling factor ν can also modify $|B|$. For $J_K > 0.01$ eV, we find that $\nu = 0$ ($N_f = 4$) yields the largest $|B|$, and $\nu = -3$ ($N_f = 1$) gives

the smallest $|B|$ as plotted in Fig. 1(b). Meanwhile, the quasiparticle dispersions along several line cuts ($K_M - \Gamma_M - M_M - K_M$) in Figs. 1(c)–1(f) show that the mini bandwidth becomes wider for a larger $|\nu|$, and no spectral gap in the low-energy bands for all the cases, suggesting symmetry-preserving correlated metallic states at all the integer fillings. The broadening of quasiparticle low-energy bands for the nonzero integer fillings is a manifestation of strong correlation [32]. We also find interaction-driven phase transitions in the quasiparticle bands of $\nu = -3$ and $\nu = -2$ [32]. Intriguingly, the $\nu = 0$ case with $|B| > 3.7$ meV gives low-energy bands very similar to the single-particle bands of MATBG [40], i.e., nearly flat isolated Dirac bands with the same bandwidth; the crucial differences are in the remote bands, particularly, the gaps between low-energy and the remote bands are proportional to $|B|$. We also point out that such low-energy bands also belong to the fragile topological bands [18–20] because of the topological equivalence to the single-particle bands. However, the physical origin here is due to strong correlations. Thus, we conclude that the Kondo lattice model realizes a fragile topological Dirac Kondo semimetal at $\nu = 0$.

So far, we have discussed the results based on the Kondo lattice model, where U is treated nonperturbatively. It is interesting to inspect the results in the perturbative regime. Following the ideas in Refs. [36,41,42], we treat the effect of $\hat{H}_U$ as a $\mathbf{k}$-independent self-energy correction on the f fermion sector. Then, we show that the quasiparticle dispersion is essentially the same as the noninteracting limit except that the cf hybridization amplitude is renormalized [32]. Therefore, the low-energy bands are also fragile topological in this perturbative analysis. We suspect the interacting MATBG generally realizes a fragile topological Dirac semimetal at $\nu = 0$.

Kondo-Heisenberg model.—One interesting question is if the Kondo semimetal ($\nu = 0$) survives perturbations. Particularly, we are interested in the competition between Kondo hybridization and magnetic correlations [43]. To this end, we consider SU(8) Heisenberg interaction among the nearest-neighbor sites given by [35]

$$\hat{H}_H = J_H \sum_{\langle \mathbf{R},\mathbf{R}'\rangle} \sum_{\substack{\alpha,\eta,s \\ \alpha',\eta',s'}} :f^\dagger_{\mathbf{R},\alpha,\eta,s} f_{\mathbf{R},\alpha',\eta',s'} :: f^\dagger_{\mathbf{R}',\alpha',\eta',s'} f_{\mathbf{R}',\alpha,\eta,s} :, \tag{11}$$

where J_H denotes the exchange coupling and $\langle \mathbf{R}, \mathbf{R}'\rangle$ indicates the nearest-neighbor pairs. Microscopically, the Heisenberg interaction may arise from RKKY and superexchange mechanisms [35]. $J_H < 0$ corresponds to a ferromagnetic interaction, and we expect that the Heisenberg ineraction with $J_H < 0$ drives the system to ground states qualitatively similar to the Hartree-Fock predictions. We thus study on the antiferromagnetic case ($J_H > 0$) and focus on the stability of the Kondo semimetal state ($\nu = 0$) in the presence of a symmetric magnetic correlation. The simplest model is a Kondo-Heisenberg Hamiltonian for MATBG, described by $\hat{H}_{0,c} + \hat{H}_K + \hat{H}_H$ with $J_H > 0$. To study the antiferromagnetic interaction, we consider a "bond" decoupling [44] as follows:

$$J_H \sum_{\substack{\alpha,\eta,s \\ \alpha',\eta',s'}} :f^\dagger_{\mathbf{R},\alpha,\eta,s} f_{\mathbf{R},\alpha',\eta',s'} :: f^\dagger_{\mathbf{R}',\alpha',\eta',s'} f_{\mathbf{R}',\alpha,\eta,s} :$$
$$\to \sum_{\alpha,\eta,s} \left[\chi_{\mathbf{R},\mathbf{R}'} f^\dagger_{\mathbf{R}',\alpha,\eta,s} f_{\mathbf{R},\alpha,\eta,s} + \text{H.c.}\right] + \frac{|\chi_{\mathbf{R},\mathbf{R}'}|^2}{J_H}, \tag{12}$$

where the bond variable

$$\chi_{\mathbf{R},\mathbf{R}'} = -J_H \sum_{\alpha,\eta,s} \left\langle f^\dagger_{\mathbf{R},\alpha,\eta,s} f_{\mathbf{R}',\alpha,\eta,s} \right\rangle. \tag{13}$$

Our goal is to explore the interplay between Kondo hybridization and magnetic correlation. In particular, we focus only on the situation without symmetry breaking as there is no clear evidence of symmetry breaking at $\nu = 0$ of MATBG. As such, we assume uniform and real-valued bond variables [35,45,46], specifically, $\chi_{\mathbf{R},\mathbf{R}'} = \chi > 0$, corresponding to a formation of a spin liquid with a spinon Fermi surface [35,47]. We note that the Kondo-Heisenberg model may give rise to a ground state different from the ansatz used here. However, our goal is to explore the interplay between symmetric Kondo hybridization and symmetric magnetic correlation, mainly, how a symmetric magnetic correlation destroys the Kondo semimetal state.

We numerically solve the Kondo-Heisenberg model with the mean-field saddle-point approximation [32] and compute the hybridization amplitude $|B|$ as well χ. In Fig. 2(a), $|B|$ as a function of J_H/J_K is plotted for a few representative values of J_K, showing the breakdown of Kondo hybridization (i.e., $|B| = 0$) for a sufficiently large J_H. In Fig. 2(b), both $|B|$ and χ are continuously varying for $J_H \leq 0.07$ eV. For $J_H > 0.07$ eV, χ continuously grows as J_H increases, while $|B|$ vanishes to zero. It is also interesting to study how quasiparticle dispersion evolves. In Fig. 3, we show the quasiparticle dispersion along

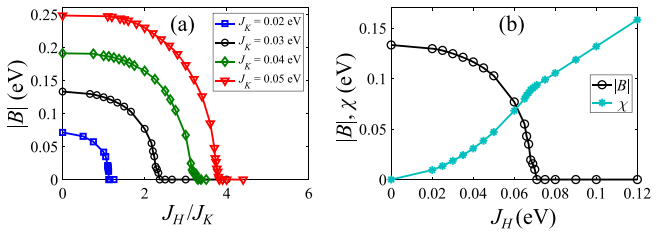

FIG. 2. Hybridization amplitude and magnetic correlation in Kondo-Heisenberg model with $N_f = 4$. (a) $|B|$ as a function of J_H/J_K for different values of J_K. (b) $|B|$ and χ as functions of J_H for $J_K = 0.03$ eV.

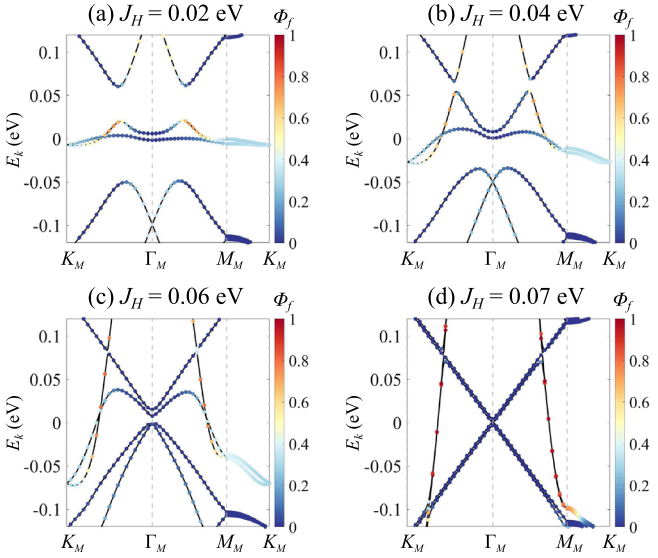

FIG. 3. Quasiparticle dispersion of the Kondo-Heisenberg model with $N_f = 4$, $J_K = 0.03$ eV, and $\eta = +1$. (a) $J_H = 0.02$ eV; (b) $J_H = 0.04$ eV; (c) $J_H = 0.06$ eV; (d) $J_H = 0.07$ eV. Φ_f is the composition of f fermion. $\Phi_f = 1$ (red) means the wave functions are made of f fermions only; $\Phi_f = 0$ (blue) indicates the wave functions are made of c fermions only.

several line cuts ($K_M - \Gamma_M - M_M - K_M$) and use the color to indicate the composition of the f fermion (Φ_f). First, we find that a small J_H [Fig. 3(a)] makes the low-energy bands wider, and the Dirac point is away from the zero energy, suggesting finite Fermi pockets around K_M and K'_M points. As J_H increases, the gaps between low-energy minibands and the remote bands decrease (as $|B|$ decreases), and the low-energy bandwidth continuously increases (as χ gives a finite dispersion). In Fig. 3(d), the quasiparticle excitations can be separated by primarily f fermions ($\Phi_f \approx 1$, red dots) and primarily c fermions ($\Phi_f \approx 0$, blue dots), indicative of a negligible $|B|$. Thus, the Fermi surface of the c fermions is reduced to a point at the Γ point for a sufficiently large J_H.

Discussion.—We establish a systematic theory for Kondo lattice models in MATBG, showing a novel route to understand the interaction-driven phenomena in MATBG. Unlike the symmetry-breaking correlated insulators predicted by Hartree-Fock calculations [21,23–31], we find symmetry-preserving correlated metals due to the Kondo coupling between a lattice of SU(8) local moments and delocalized electrons. The Kondo lattice description in this Letter may be relevant to the MATBG experiments at $\nu = 0$. In particular, the STM measurements concluded the existence of strong correlations at $\nu = 0$ [9,10,14,17], while several transport measurements [1,2,4,15] did not find a clear sign of symmetry breaking or correlated insulating behavior. Our predicted Dirac Kondo semimetal state potentially explains the dichotomy [48] of strong correlation and the symmetry-preserving Dirac point. Our theory also complements the existing list of Kondo lattice systems in the moiré materials [49–52] and extends the number of topological phases driven by Kondo correlation [43,53–59].

One interesting consequence of our results is that the local moments (i.e., f fermions) can be decoupled entirely from the c fermions by a sufficiently strong magnetic correlation, paving the way for realizing a quantum simulator for a SU(8) triangular Heisenberg model in MATBG. The SU(N) magnetic systems with $N > 2$ can realize exotic phases, such as spin liquids and valence bond solids [60–65]. The ground states of SU(8) triangular Heisenberg model have not been systematically explored (except for $N_f = 1$ [65]), and our work provides a strong incentive for future studies along this direction.

An outstanding question is whether the Kondo lattice model and Kondo-driven correlated states are relevant to the realistic MATBG. Using the parameters in Ref. [21], we obtain $U/|\gamma| \approx 2.34$, indicating that the system is in the intermediate coupling regime. Thus, the Kondo lattice models based on the strong-coupling analysis (i.e., $U/|\gamma| \gg 1$) might not explain all the experimental results. Our predicted Dirac Kondo semimetal is consistent with several existing experiments at $\nu = 0$, introducing a new perspective to study MATBG [66]. On the contrary, at nonzero integer fillings, the Kondo-driven correlated metals cannot explain various symmetry-broken states from experiments. It is possible that other types of interaction-driven states (e.g., correlated insulators) are more energetically favored. Further investigations are required to determine if Kondo-driven correlated states can be realized in the MATBG experiments. Regardless of these complications, our predicted Kondo-driven semimetal provides a plausible novel explanation for semimetallic transport of MATBG at $\nu = 0$.

Finally, we discuss a few open questions. In the Kondo-Heisenberg model, we consider a specific magnetic correlation and $J_H > 0$. The actual ground state with a finite J_K and J_H should be examined systematically. In particular, for $J_H < 0$, we anticipate that the ground states are qualitatively similar to the Hartree-Fock predictions (e.g., valley-polarized states) [21,23–31]. It might be interesting to study our Kondo-Heisenberg model with $J_H < 0$ for nonzero integer fillings, where symmetry-broken states are reported experimentally. An important task is to compute observables that can reveal the finite-temperature crossover between the coherent Kondo lattice and the decoupled Kondo impurities, such as temperature-dependent tunneling spectroscopy and finite-temperature resistivity.

Y.-Z. C. thanks Seth Davis, Zhentao Wang, Fengcheng Wu, Ming Xie, Jiabin Yu, and Rui-Xing Zhang for useful discussions. This work is supported by the Laboratory for

Physical Sciences (Y.-Z. C. and S. D. S.), by JQI-NSF-PFC (Y.-Z. C.), and by ARO W911NF2010232 (Y.-Z. C.).

Note added.—Recently, we learned that related results have also recently been obtained by another group (Hu *et al.*) [67].

*yzchou@umd.edu

[1] Y. Cao, V. Fatemi, A. Demir, S. Fang, S. L. Tomarken, J. Y. Luo, J. D. Sanchez-Yamagishi, K. Watanabe, T. Taniguchi, E. Kaxiras *et al.*, Nature (London) **556**, 80 (2018).

[2] Y. Cao, V. Fatemi, S. Fang, K. Watanabe, T. Taniguchi, E. Kaxiras, and P. Jarillo-Herrero, Nature (London) **556**, 43 (2018).

[3] R. Bistritzer and A. H. MacDonald, Proc. Natl. Acad. Sci. U.S.A. **108**, 12233 (2011).

[4] M. Yankowitz, S. Chen, H. Polshyn, Y. Zhang, K. Watanabe, T. Taniguchi, D. Graf, A. F. Young, and C. R. Dean, Science **363**, 1059 (2019).

[5] A. Kerelsky, L. J. McGilly, D. M. Kennes, L. Xian, M. Yankowitz, S. Chen, K. Watanabe, T. Taniguchi, J. Hone, C. Dean *et al.*, Nature (London) **572**, 95 (2019).

[6] X. Lu, P. Stepanov, W. Yang, M. Xie, M. A. Aamir, I. Das, C. Urgell, K. Watanabe, T. Taniguchi, G. Zhang *et al.*, Nature (London) **574**, 653 (2019).

[7] A. L. Sharpe, E. J. Fox, A. W. Barnard, J. Finney, K. Watanabe, T. Taniguchi, M. Kastner, and D. Goldhaber-Gordon, Science **365**, 605 (2019).

[8] M. Serlin, C. Tschirhart, H. Polshyn, Y. Zhang, J. Zhu, K. Watanabe, T. Taniguchi, L. Balents, and A. Young, Science **367**, 900 (2020).

[9] Y. Jiang, X. Lai, K. Watanabe, T. Taniguchi, K. Haule, J. Mao, and E. Y. Andrei, Nature (London) **573**, 91 (2019).

[10] Y. Xie, B. Lian, B. Jäck, X. Liu, C.-L. Chiu, K. Watanabe, T. Taniguchi, B. A. Bernevig, and A. Yazdani, Nature (London) **572**, 101 (2019).

[11] H. Polshyn, M. Yankowitz, S. Chen, Y. Zhang, K. Watanabe, T. Taniguchi, C. R. Dean, and A. F. Young, Nat. Phys. **15**, 1011 (2019).

[12] Y. Cao, D. Chowdhury, D. Rodan-Legrain, O. Rubies-Bigorda, K. Watanabe, T. Taniguchi, T. Senthil, and P. Jarillo-Herrero, Phys. Rev. Lett. **124**, 076801 (2020).

[13] J. M. Park, Y. Cao, K. Watanabe, T. Taniguchi, and P. Jarillo-Herrero, Nature (London) **592**, 43 (2021).

[14] Y. Choi, J. Kemmer, Y. Peng, A. Thomson, H. Arora, R. Polski, Y. Zhang, H. Ren, J. Alicea, G. Refael *et al.*, Nat. Phys. **15**, 1174 (2019).

[15] U. Zondiner, A. Rozen, D. Rodan-Legrain, Y. Cao, R. Queiroz, T. Taniguchi, K. Watanabe, Y. Oreg, F. von Oppen, A. Stern *et al.*, Nature (London) **582**, 203 (2020).

[16] H. S. Arora, R. Polski, Y. Zhang, A. Thomson, Y. Choi, H. Kim, Z. Lin, I. Z. Wilson, X. Xu, J.-H. Chu *et al.*, Nature (London) **583**, 379 (2020).

[17] D. Wong, K. P. Nuckolls, M. Oh, B. Lian, Y. Xie, S. Jeon, K. Watanabe, T. Taniguchi, B. A. Bernevig, and A. Yazdani, Nature (London) **582**, 198 (2020).

[18] Z. Song, Z. Wang, W. Shi, G. Li, C. Fang, and B. A. Bernevig, Phys. Rev. Lett. **123**, 036401 (2019).

[19] H. C. Po, L. Zou, T. Senthil, and A. Vishwanath, Phys. Rev. B **99**, 195455 (2019).

[20] J. Ahn, S. Park, and B.-J. Yang, Phys. Rev. X **9**, 021013 (2019).

[21] Z.-D. Song and B. A. Bernevig, Phys. Rev. Lett. **129**, 047601 (2022).

[22] J. Liu, J. Liu, and X. Dai, Phys. Rev. B **99**, 155415 (2019).

[23] H. Shi and X. Dai, Phys. Rev. B **106**, 245129 (2022).

[24] M. Xie and A. H. MacDonald, Phys. Rev. Lett. **124**, 097601 (2020).

[25] Y. Zhang, K. Jiang, Z. Wang, and F. Zhang, Phys. Rev. B **102**, 035136 (2020).

[26] N. Bultinck, E. Khalaf, S. Liu, S. Chatterjee, A. Vishwanath, and M. P. Zaletel, Phys. Rev. X **10**, 031034 (2020).

[27] J. Liu and X. Dai, Phys. Rev. B **103**, 035427 (2021).

[28] B. A. Bernevig, Z.-D. Song, N. Regnault, and B. Lian, Phys. Rev. B **103**, 205413 (2021).

[29] B. Lian, Z.-D. Song, N. Regnault, D. K. Efetov, A. Yazdani, and B. A. Bernevig, Phys. Rev. B **103**, 205414 (2021).

[30] B. A. Bernevig, B. Lian, A. Cowsik, F. Xie, N. Regnault, and Z.-D. Song, Phys. Rev. B **103**, 205415 (2021).

[31] G. Wagner, Y. H. Kwan, N. Bultinck, S. H. Simon, and S. A. Parameswaran, Phys. Rev. Lett. **128**, 156401 (2022).

[32] See Supplemental Material at http://link.aps.org/supplemental/10.1103/PhysRevLett.131.026501 for derivations and extended discussions.

[33] We focus only on the single-particle bands relevant to MATBG experiment (corresponding to $w_0/w_1 = 0.8$, $w_1 = 110$ meV, and $\theta = 1.05°$ in the BM model). In the chiral limit ($w_0 = 0$ in the BM model), the f orbitals are much less localized, resulting in a U much smaller than the cf hybridization [21].

[34] The nearest-neighbor interaction is an order of magnitude smaller than the onsite term [21].

[35] P. Coleman, *Introduction to Many-Body Physics* (Cambridge University Press, Cambridge, England, 2015), ISBN 9780521864886.

[36] A. C. Hewson, *The Kondo Problem to Heavy Fermions*, (Cambridge University Press, Cambridge, England, 1997).

[37] The normal ordering is given by: $\hat{A}: \equiv A - \langle G|A|G\rangle$, where $\langle G|c^\dagger_{\mathbf{q},a,\eta,s}c_{\mathbf{q},a',\eta',s'}|G\rangle = \frac{1}{2}\,\delta_{\mathbf{q},\mathbf{q}'}\delta_{a,a'}\delta_{\eta,\eta'}\delta_{s,s'}$, $\langle G|f^\dagger_{\mathbf{k},\alpha,\eta,s}f_{\mathbf{k},\alpha',\eta',s'}|G\rangle = \frac{1}{2}\,\delta_{\mathbf{k},\mathbf{k}'}\delta_{\alpha,\alpha'}\delta_{\eta,\eta'}\delta_{s,s'}$, and $\langle G|f^\dagger_{\mathbf{k},\alpha,\eta,s}c_{\mathbf{q},a',\eta',s'}|G\rangle = 0$.

[38] B. Coqblin and J. R. Schrieffer, Phys. Rev. **185**, 847 (1969).

[39] N. Read and D. Newns, J. Phys. C **16**, 3273 (1983).

[40] For $|B| < 3.7$ meV, the minibands are not isolated. See Ref. [32] for a discussion.

[41] D. Edwards, in *Narrow-Band PhenomenaInfluence of Electrons with Both Band and Localized Character* (Springer, New York, 1988), pp. 23–26.

[42] K. Yamada and K. Yosida, Prog. Theor. Phys. **76**, 621 (1986).

[43] S. Paschen and Q. Si, Nat. Rev. Phys. **3**, 9 (2021).

[44] X.-G. Wen, *Quantum Field Theory of Many-Body Systems: From the Origin of Sound to an Origin of Light and Electrons* (Oxford University Press, Oxford, 2004).

[45] S. Saremi and P. A. Lee, Phys. Rev. B **75**, 165110 (2007).

[46] H. Hu and Q. Si, arXiv:2209.10396.

[47] Y.-D. Li, Y.-M. Lu, and G. Chen, Phys. Rev. B **96**, 054445 (2017).
[48] A. Thomson and J. Alicea, Phys. Rev. B **103**, 125138 (2021).
[49] A. Kumar, N. C. Hu, A. H. MacDonald, and A. C. Potter, Phys. Rev. B **106**, L041116 (2022).
[50] A. Ramires and J. L. Lado, Phys. Rev. Lett. **127**, 026401 (2021).
[51] D. Guerci, J. Wang, J. Zang, J. Cano, J. Pixley, and A. Millis, Sci. Adv. **9**, eade7701 (2023).
[52] W. Zhao, B. Shen, Z. Tao, Z. Han, K. Kang, K. Watanabe, T. Taniguchi, K. F. Mak, and J. Shan, Nature (London) **616**, 61 (2023).
[53] M. Dzero, K. Sun, V. Galitski, and P. Coleman, Phys. Rev. Lett. **104**, 106408 (2010).
[54] M. Dzero, J. Xia, V. Galitski, and P. Coleman, Annu. Rev. Condens. Matter Phys. **7**, 249 (2016).
[55] P.-Y. Chang, O. Erten, and P. Coleman, Nat. Phys. **13**, 794 (2017).
[56] J. H. Pixley, S. B. Lee, B. Brandom, and S. A. Parameswaran, Phys. Rev. B **96**, 081105(R) (2017).
[57] H.-H. Lai, S. E. Grefe, S. Paschen, and Q. Si, Proc. Natl. Acad. Sci. U.S.A. **115**, 93 (2018).
[58] S. E. Grefe, H.-H. Lai, S. Paschen, and Q. Si, Phys. Rev. B **101**, 075138 (2020).
[59] L. Chen, C. Setty, H. Hu, M. G. Vergniory, S. E. Grefe, L. Fischer, X. Yan, G. Eguchi, A. Prokofiev, S. Paschen *et al.*, Nat. Phys. **18**, 1341 (2022).
[60] D. S. Rokhsar, Phys. Rev. B **42**, 2526 (1990).
[61] M. Hermele, V. Gurarie, and A. M. Rey, Phys. Rev. Lett. **103**, 135301 (2009).
[62] A. V. Gorshkov, M. Hermele, V. Gurarie, C. Xu, P. S. Julienne, J. Ye, P. Zoller, E. Demler, M. D. Lukin, and A. Rey, Nat. Phys. **6**, 289 (2010).
[63] M. Hermele and V. Gurarie, Phys. Rev. B **84**, 174441 (2011).
[64] Y.-H. Zhang, D. N. Sheng, and A. Vishwanath, Phys. Rev. Lett. **127**, 247701 (2021).
[65] X.-P. Yao, Y. Gao, and G. Chen, Phys. Rev. Res. **3**, 023138 (2021).
[66] There are also some experiments that support correlated insulated states at $\nu = 0$ [6]. The semimetallicity versus gap situation is likely due to the twist-angle disorder, moiré potential from hexagonal boron nitride, and so on. In this work, we provide a theory for the semimetallic transport behavior at $\nu = 0$.
[67] H. Hu, B. A. Bernevig, and A. M. Tsvelik, following Letter, Phys. Rev. Lett. **131**, 026502 (2023).